



RESEARCH LETTER

10.1029/2018GL080412

Key Points:

- We present the first spaceborne GNSS radio occultation signals acquired at two polarizations
- The measured observables sense intense precipitation and capture its vertical structure
- No other technique captures both thermodynamics and hydrometeor profiling in intense rain phenomena

Supporting Information:

- Supporting Information S1

Correspondence to:

E. Cardellach,
estel@ice.csic.es

Citation:

Cardellach, E., Oliveras, S., Rius, A., Tomás, S., Ao, C. O., Franklin, G. W., et al. (2019). Sensing heavy precipitation with GNSS polarimetric radio occultations. *Geophysical Research Letters*, 46, 1024–1031. <https://doi.org/10.1029/2018GL080412>

Received 9 SEP 2018
Accepted 11 DEC 2018
Accepted article online 21 DEC 2018
Published online 22 JAN 2019

Sensing Heavy Precipitation With GNSS Polarimetric Radio Occultations

E. Cardellach^{1,2}, S. Oliveras^{1,2}, A. Rius^{1,2}, S. Tomás^{1,2}, C. O. Ao³, G. W. Franklin³, B. A. Iijima³, D. Kuang³, T. K. Meehan³, R. Padullés³, M. de la Torre Juárez³, F. J. Turk³, D. C. Hunt⁴, W. S. Schreiner⁴, S. V. Sokolovskiy⁴, T. Van Hove⁴, J. P. Weiss⁴, Y. Yoon⁴, Z. Zeng⁴, J. Clapp⁵, W. Xia-Serafino⁵, and F. Cerezo⁶

¹Institute of Space Sciences (ICE, CSIC), Barcelona, Spain, ²Institute for Space Studies of Catalonia (IEEC), Barcelona, Spain, ³Jet Propulsion Laboratory, California Institute of Technology, Pasadena, CA, USA, ⁴University Corporation for Atmospheric Research, Boulder, CO, USA, ⁵National Oceanic and Atmospheric Administration, Silver Spring, MD, USA, ⁶Hisdesat, Madrid, Spain

Abstract This study presents, for the first time ever, occulting signals of the Global Navigation Satellite Systems (GNSSs) acquired at two polarizations from a Low Earth Orbiter, and it shows that they sense heavy precipitation. The data sets are obtained from early stages of the Radio Occultation and Heavy Precipitation experiment aboard the PAZ satellite, launched in February 2018 and activated in May 2018. Preliminary calibration algorithms are applied to remove other systematic effects, and the resulting vertical profiles of polarimetric phase shift observations are compared to precipitation information from other missions. The analysis of the data shows consistency between Radio Occultation and Heavy Precipitation experiment aboard the PAZ satellite polarimetric phase shift measurements and presence of hydrometeors, with strong signatures from heavy precipitation. The polarimetric measurements also capture vertical features consistent with the vertical structures of precipitation.

Plain Language Summary When the satellites of the navigation systems (like GPS) set below the horizon, their signals can be used to measure temperature, pressure, and humidity of the atmosphere at different altitudes (an observation called radio occultation). For the first time, a satellite has collected these setting GPS signals at two polarizations, that is, separating two different orientations of the electromagnetic field (horizontal and vertical with respect to the receiving antenna). It is the Radio Occultation and Heavy Precipitation experiment aboard PAZ satellite, launched in February 2018 and activated in May 2018. Previous theoretical studies have shown that intense rain crossing the path of the GPS signals would introduce a delay of the horizontal component with respect to the vertical one. This study shows the analysis of the polarimetric delays, and it confirms that they are related to the presence of rain, in particular intense precipitation. The measurement of polarimetric delays at different altitudes is consistent with the presence of rain structures at different heights. No other technique captures profiles of both thermodynamics and hydrometeor content in intense rain phenomena, and therefore, the Radio Occultation and Heavy Precipitation experiment aboard the PAZ satellite data could provide a new tool to understand extreme precipitation, with potential to improve its difficult prediction.

1. Introduction

Heavy precipitation events have severe impacts on human life and property, representing one of the main sources of billion-dollar disasters (Smith & Katz, 2013). The most recent decadal survey for Earth Science, sponsored by the National Aeronautics and Space Administration, National Oceanic and Atmospheric Administration, and U.S. Geological Survey, identified improvements in precipitation prediction as a primary objective (NASEM: National Academies of Sciences Engineering and Medicine, 2018). The driver of the most intense precipitation is convection, the process by which rapidly rising buoyant air carries moisture from near the Earth's surface upward, condensing to produce precipitation. Unfortunately, convection is poorly understood globally and limits the ability of forecast and climate models to accurately predict and represent precipitation, respectively (Intergovernmental Panel on Climate Change, 2014; Sherwood et al., 2013; Zhao et al., 2016).

©2018. The Authors.
This is an open access article under the terms of the Creative Commons Attribution-NonCommercial-NoDerivs License, which permits use and distribution in any medium, provided the original work is properly cited, the use is non-commercial and no modifications or adaptations are made.

There are no current missions or instruments capable of directly observing vertically resolved information in and near convection to address fundamental questions related to the role of water vapor structure in initiating heavy precipitation events (Kuo et al., 2017; Schiro et al., 2016). The processes within the convection are dependent on the environment—the water vapor and temperature vertical profiles in the region surrounding the convection. Low Earth orbiting satellite-based passive microwave sounding radiometers such as the Advanced Technology Microwave Sounder operate in millimeter-wave water vapor bands, which under heavy precipitation are sensitive to the upper cloud ice region (Haddad et al., 2017). Microwave imaging radiometers such as the Global Precipitation Measurement (GPM) Microwave Radiometer provide total column water vapor over ocean (Duncan & Kummerow, 2016). From precipitation profiling radars such as the GPM Dual-Frequency Precipitation Radar (DPR), the water vapor and precipitation profile cannot be separated solely from the radar backscattered signal.

Polarimetric radio occultation (PRO) measurements have been proposed as a method to characterize heavy rain in Global Navigation Satellite System (GNSS) radio occultations (ROs), by measuring its thermodynamic vertical structure (usual GNSS RO application, e.g., Anthes et al., 2008; Kursinski et al., 1997) while simultaneously acquiring the polarimetric differential phase delay induced by large size asymmetric hydrometeors, which links to the rain rate. The Radio Occultation and Heavy Precipitation aboard PAZ (ROHP-PAZ) is a spaceborne experiment to prove the PRO concept. It consists of a GNSS receiver tuned to acquire signals at two linear polarizations (horizontal and vertical components) as provided by a dual polarization antenna pointing to the limb of the Earth, under radio occultation geometry. The receiver is the same as in the COSMIC/FORMOSAT-3 mission, providing similar performances. Further details of the mission, PRO instrument, and initial sensitivity studies are described in Cardellach et al. (2014), Padullés et al. (2016), and Padullés et al. (2016), while the theoretical base and intended retrieval algorithms can be found in Tomás et al. (2018) and Cardellach et al. (2017), respectively. These theoretical studies show that precipitation induces GNSS PRO signals above the expected noise levels and with systematic effects in principle removable. The PAZ satellite was launched in February 2018, and the ROHP-PAZ experiment is operating since mid-May 2018. The mission is currently in commissioning phase, including system calibration and validation. The early data reported in this study present clear sensitivity to intense precipitation. After the commissioning phase, levels 1 and 2 data (observables and geophysical retrievals, respectively) will be made publicly available for research purposes during PAZ lifetime (over 5 years nominal lifetime).

2. Data Set

We analyze ROHP-PAZ GNSS PRO profiles obtained over 5 months, from 10 May to 10 October 2018. Being part of the commissioning phase, a few changes in configuration and operational tests were run during the acquisition period, reducing the total amount of otherwise available data. The total number of profiles collected for the period was 27,034. For analysis purposes, these profiles have been colocated with the IMERG (Integrated Multi-satellitE Retrievals for GPM) products, which intercalibrate, merge, and interpolate several satellite passive microwave precipitation estimates, together with microwave-calibrated infrared satellite estimates, monthly precipitation gauge analyses, among others (Huffman et al., 2015; Huffman, 2017), and with infrared brightness temperatures as provided in the NCEP/CPC Merged IR products, sourced from different satellites (Janowiak et al., 2017). IMERG rain rate products are used here as an indicator of precipitation but cannot be used as a calibration reference because they are surface fields (2-D) without direct information on the vertical structures of the precipitating cells. Three-dimensional (3-D) information would be required to properly compare to the altitude-dependent limb sounding geometry of GNSS RO. Moreover, the performance of IMERG varies over different surfaces (e.g., ocean/land), and it has its own limitations. For example, Tan et al. (2017) found that IMERG misses detection in 8% of the cases and it yields false positives in another 5.5% at resolutions of 0.5 hr over 2°. The maximum time separation between ROHP-PAZ and the ancillary products is required to be 15 min, and they have been averaged around the location of the RO profile (here defined as the average location of the RO tangent points in the lowest third of its profile). These products are averaged to deal with the fact that (1) the ROHP-PAZ observation represents an integration along its raypath and (2) in this study the actual orientation of the ROHP-PAZ observation is not considered.

Two averaging schemes have been used in this study: mean across cells of size equivalent to the size of a 2° longitude × 2° latitude cell in the equator (identified hereafter by subscript 2°, e.g., averaged IMERG rain rate $\langle R_{\text{IMERG}} \rangle_{2^\circ} \times 2^\circ \equiv R_{2^\circ}$) and similarly across 0.6° × 0.6° cells (subscript 0.6°). The size of the two averaging cells complements each other: 2° is similar to the distance traveled by the ROHP-PAZ rays at the bottom layers

(where precipitation occurs), making sure the significant segment of the ray is within the cell, although rain might be present in other areas of the cell not actually crossed by the ray. The chance that the rain within the cell is actually crossed by the RO rays increases by averaging over a smaller area, such as $0.6^\circ \times 0.6^\circ$, but then some rain crossed by the rays might have been left outside the smaller cell. Both schemes introduce inaccuracies in the collocation that increase the dispersion of the analysis. These inaccuracies have to be added to the dispersion introduced by the performance of IMERG over these spatiotemporal resolutions ($\sim 14\%$ failures; Tan et al., 2017). The IMERG grid covers from -60° to 60° latitude; therefore, a significant number of ROHP-PAZ profiles do not have colocated IMERG information, and they are not analyzed in this study. The quality controls applied to the individual H-pol and V-pol profiles are based on (a) their successful inversion to vertical profiles of refractivity, temperature, and water vapor and (b) the retrieved refractivity profiles must be within 10% of the colocated NCEP/GFS analysis from 0- to 30-km altitude. We also remove profiles without data below 20 km and those with data only below 20 km. The number of colocated profiles that have passed the quality control are 14,297 with 4,338 of them presenting some rain within the equator-equivalent $2^\circ \times 2^\circ$ cell around the profile (see their geographic distribution in supporting information S1).

3. ROHP-PAZ Data Processing

The ROHP-PAZ data for each occultation primarily consist of time series of GNSS signal amplitude and carrier-phase delay as the GNSS transmitter sets below the horizon. Only GPS L1 signals have been analyzed (~ 1.5 GHz). Traditionally, from the excess phase delay (with respect to vacuum propagation) it is possible to determine the bending suffered by the radio link as induced by vertical gradients of the atmosphere, from which vertical profiles of the refractive index (temperature, pressure, and moisture) are inferred (e.g., Kursinski et al., 1997). These type of observables and retrievals are used in this study for quality control and to help estimating the cloud top height (CTH). The analysis is instead focused on the novel polarimetric effects of the ROHP-PAZ. The new observables are the polarimetric phase shift, or relative phase delay between H-polarized signals with respect to the V-polarized ones. As detailed in Tomás et al. (2018), hydrometeors are not the only effect inducing polarimetric phase shift, but other factors also induce these phase delays: the GNSS transmitter polarization purity, Faraday rotations (ionosphere and magnetic field), antenna phase pattern, instrumental delays, and an arbitrary initial phase with which the receiver starts the measurements at each polarization channel. During commissioning phase, all these effects are being characterized and calibration strategies are being analyzed. A simple calibration approach is used in this study, as reported in the fifth and sixth points below. Note that some residual effects might have not yet been properly removed. Starting from excess phase delay observables interpolated at common acquisition times for H- and V-polarized signals, the processing steps are as follows:

1. At every observational time, subtract the phase delay of V-polarized signals from the delay of the H-polarized one: $\Delta\phi_1(t) = \phi_H(t) - \phi_V(t)$.
2. Remove an offset equal to the first value of the time series: $\Delta\phi_2(t) = \Delta\phi_1(t) - \Delta\phi_1(t_0)$.
3. Remove any remaining cycle slip appearing in $\Delta\phi_2(t)$.
4. Express the time series as a function of the altitude of the radio link tangent point: $\Delta\phi_2(h_t) = \Delta\phi_2(h_t(t))$. This step is based on the traditional RO retrievals.
5. Fit a linear trend onto the segment of data between 20- and 70-km altitude: $\Delta\phi_m(h_t) \sim a + bh_t$. The trend is due to nonhydrometeor systematic effects (transmitted ellipticity, Faraday rotations, antenna phase pattern, and instrumental delays), and it was described and tested with synthetic data in Tomás et al. (2018).
6. Correct the entire profile, down to the bottom layer, with the linear trend: $\Delta\phi(h_t) = \Delta\phi_2(h_t) - (a + bh_t)$.
7. Filter at 1 Hz to reduce noise. This last step reduces the vertical resolution, which at the bottom layers of the troposphere becomes approximately a few hundred meters.

An example of the result of this process is shown in Figure 1, for a case partially colocated with GPM orbital products (Grecu et al., 2016) within 7-min mismatch. The ROHP-PAZ $\Delta\phi(h_t)$ observation shows a positive differential phase shift that agrees reasonably well with the 3-D precipitation structure, despite the limitations of the collocation. Here we present the polarimetric shift in degrees instead of millimeter delay (units of length used by the GNSS community), to avoid confusion with the units of precipitation (mm, mm/hr). The conversion factor to return the phase shift from degree to GPS L1 millimeter phase delay, used in the previous GNSS PRO studies, is $\lambda_{mm}^{L1}/360^\circ = 0.528$.

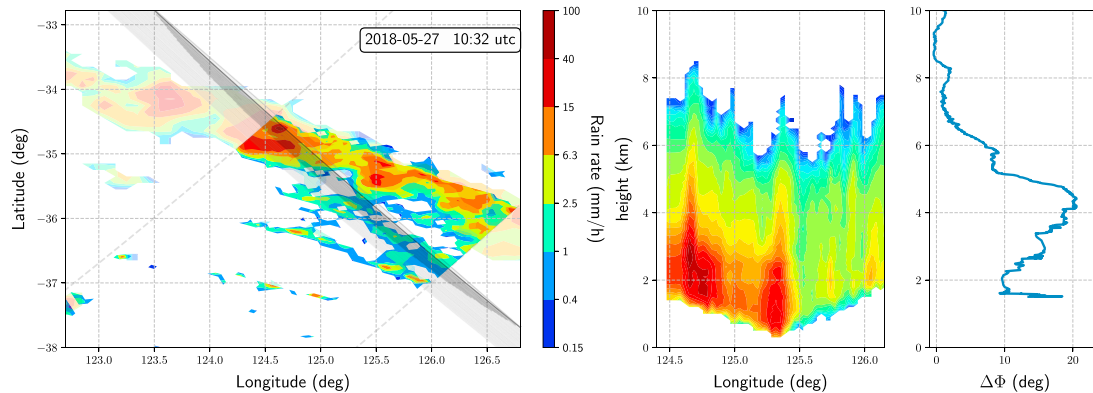


Figure 1. ROHP-PAZ profile partially colocated with GPM DPR 3-D precipitation products (Greco et al., 2016; Olson, 2017), and resulting polarimetric phase shift: (left) maximum columnar rain rate provided by the GPM radar projected onto the surface (solid color between dashed lines) and the different ROHP-PAZ ray trajectories in gray (light gray for ray points at altitudes above 10 km and dark gray otherwise). The tangent (central) points of the RO lay approximately around longitude 124.5°. Semitransparent colors beyond the dashed lines correspond to precipitation information obtained from the GPM radiometer (GMI), which does not provide vertical structure; (middle) vertical precipitation structure as measured along GPM DPR slices interpolated to the ROHP-PAZ observational planes and adjacent to them (± 50 km). Only the maximum rain rates at each longitude are shown. GPM GMI data are not included in this panel because of their lack of vertical information. Approximately half of the RO plane misses 3-D rain information due to the orientation of the RO plane relative to the DPR swath; and (right) the differential phase shift $\Delta\phi(h_t)$ observed by ROHP-PAZ. ROHP-PAZ = Radio Occultation and Heavy Precipitation aboard PAZ; GPM = Global Precipitation Measurement; DPR = Dual-Frequency Precipitation Radar; GMI = GPM Microwave Radiometer.

4. Is ROHP-PAZ Sensing Heavy Precipitation?

The collocation between ROHP-PAZ profiles and IMERG gridded data is used to separate the profiles occurring under rain-free conditions from those occurring under potential precipitation. The use of IMERG has the advantage of providing gridded products with fine temporal resolutions (30-min batches), but the main disadvantage is the lack of 3-D information, which would enable the comparison with vertical structures in ROHP-PAZ. For the purpose of testing sensitivity to precipitation, it is enough to base the spatial collocation on IMERG rain rate products averaged across the larger cells around the ROHP-PAZ events (R_{2°). For complementarity, in certain cases we have also used the mean IMERG values averaged across the smaller cells ($R_{0.6^\circ}$). The statistics of the polarimetric phase shift at different altitudes are computed for two data subsets separately: the rain-free events and the rain events (Figure 2): the profiles occurring under rain-free conditions average to zero at most altitudes, except a small positive bias of $\sim 1^\circ$ near the surface level. The dispersion of $\Delta\phi$ is smaller than 2° above 4.5-km altitude, and it is better than 4° on the surface level. The former study in Cardellach et al. (2014) anticipated values of this order of magnitude (2.8° noise at the surface level, improving with altitude). The ROHP-PAZ performance is slightly worse, likely related to near-field effects provoked by a large metallic ring close to the RO antenna, a mechanical interface that had to be assembled months before launch to adapt the satellite to a change of launcher and that distorts the antenna pattern reducing the signal-to-noise level of the signals over certain angular ranges. The slightly increased dispersion could also be due to small interpolation errors when aligning H and V signals to common time tags. Regarding the small positive bias, it is being studied in terms of possible ionospheric (e.g., Faraday rotation) and instrumental effects. At the moment, the main component of the bias seems unrelated to the ionosphere, while it shows dependency on the azimuth angle in the antenna reference frame. This might be an indication that ancillary calibration of antenna effects need to be conducted and data accordingly corrected. This bias may also be related to effects of low SNR (Sokolovskiy et al., 2010) as well as independent tracking of H and V signals (Cardellach et al., 2014). These possibilities will be further investigated. False negative collocations (rain events flagged as rain free) could also contribute to the positive bias. In contrast, the set of ROHP-PAZ profiles acquired under rain conditions present clear offsets toward positive values, its mean exceeding the dispersion of the rain-free statistics in most altitudes. This implies a statistically significant signal. The dispersion of the set of rainy events is much larger, as it captures the different magnitudes for different rain events and inaccuracies of the collocation.

The statistics shown in the left and middle panels of Figure 2 have been computed analyzing all the profiles at each altitude. Nonetheless, the near-zero mean found for rain-free events does not guarantee that each of the individual profiles averages to zero (profiles biased in opposite directions would average out the mean values in Figure 2, left). To check the performance of individual profiles, the mean polarimetric phase shift of

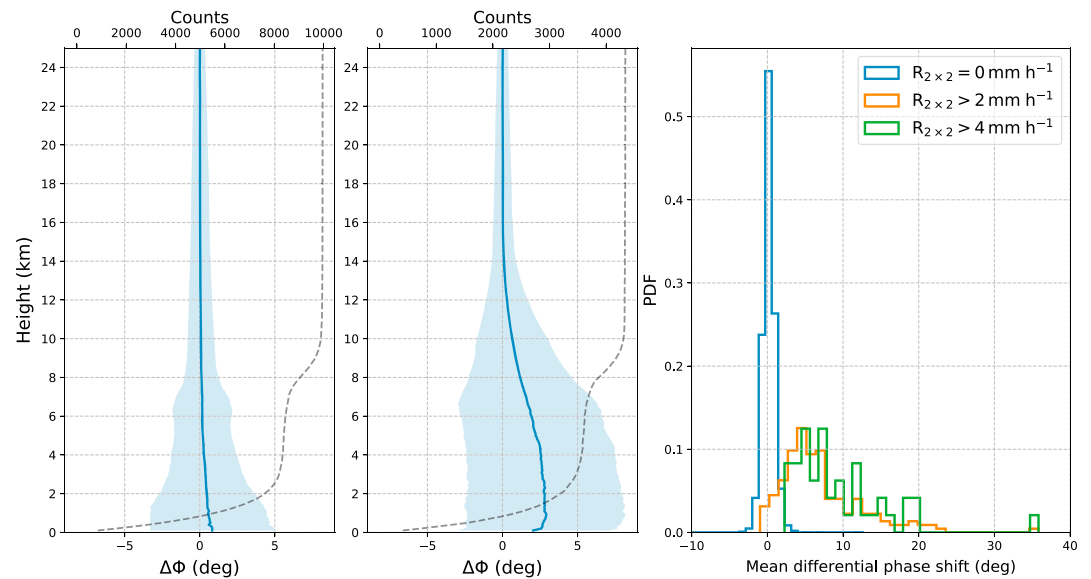


Figure 2. Mean and standard deviation of Radio Occultation and Heavy Precipitation aboard PAZ profiles at different altitudes (left) under rain-free conditions and (middle) under rain condition of any intensity. Upper axis and dashed line for the number of cases. See supporting information S1 for the geographical distribution of the rainy events. Right: Histograms of the individual profiles' $\langle \Delta\phi \rangle_{0-20\text{km}}$ under rain-free condition (blue, 9,959 profiles), $R_{2^{\circ}} > 2$ mm/hr (orange, 187 profiles) and $R_{2^{\circ}} > 4$ mm/hr (green, 43 profiles). More information on the extreme case with $\langle \Delta\phi \rangle_{0-20\text{km}} \sim 35^{\circ}$ shift can be found in supporting information S2.

each of them, evaluated under 20 km only, has been generated, $\langle \Delta\phi \rangle_{0-20\text{km}}$. Histograms of $\langle \Delta\phi \rangle_{0-20\text{km}}$ are shown in Figure 2 (right). The 98.4% and 99.97% of the rain-free events have a mean polarimetric phase shift smaller than 2° and 4° , respectively. The histogram shifts toward larger positive values for rainy events. Nearly no overlap is found between rain-free profiles and those with averaged rain rates larger than $R_{2^{\circ}} > 4$ mm/hr. A threshold defined as $\langle \Delta\phi \rangle_{0-20\text{km}} \geq 4^{\circ}$ for intense rain events results in $< 1\%$ of false positives, but some would remain undetected (e.g., three events with $R_{2^{\circ}} > 4$ mm/hr in this data set). These thresholds and percentages are provided to illustrate the link between the observable $\Delta\phi$ and hydrometeors, but at this stage they are not understood as the thresholds of an actual detection algorithm. More data over different seasons are needed before we can establish skill score metrics as a function of the detection threshold. The relationship between the mean rain rate within the cell and the mean polarimetric shift is presented in Figure 3, where $\langle \Delta\phi \rangle_{0-20\text{km}}$ clearly increases with rain rate. This supports the hypothesis that GNSS PRO senses rain, with larger response from intense precipitation.

During the 5-month period analyzed in this study, 98 ROHP-PAZ profiles are spatiotemporally collocated with GPM DPR 3-D products (Olson, 2017) between $\pm 60^{\circ}$ latitude. Among them, only four present intense rain, but the collocation is marginal in three of them. Figure 1 presents one of the GPM DPR 3-D collocations with larger overlap. This quantity is insufficient at the moment to check whether the vertical structures of the ROHP-PAZ polarimetric phase shift are consistent with the vertical distribution of hydrometeors. For this reason we have used the CTH as indicator of the vertical extension of the observed systems. We estimate CTH as the altitude of the ROHP-PAZ RO temperature profile that matches the infrared brightness temperature (Holz et al., 2006). While this CTH is not necessarily accurate under all circumstances, we assume that, on average, it will act as an indicator of higher versus lower hydrometeors. Figure 4 (left) presents the vertical statistics of events for which IMERG rain rates $R_{2^{\circ}}$ exceed 1 mm/hr, grouping them as a function of the estimated CTH. The statistics present polarimetric shift features at higher altitudes for events within higher clouds, peaking around ~ 7 -km altitude when the CTH is above 13 km, while $\Delta\phi$ in lower clouds present maximum polarimetric shifts at around ~ 2.5 km. This is consistent with the presence of hydrometeors at higher and lower layers of the troposphere. To check whether humidity could also explain these vertical structures, Figure 4 (middle) presents the mean and dispersion of the humidity as a function of the altitude for the same data sets. The plots show that the vertical humidity profile does not match the structure of the polarimetric phase shift measurements; thus, it cannot

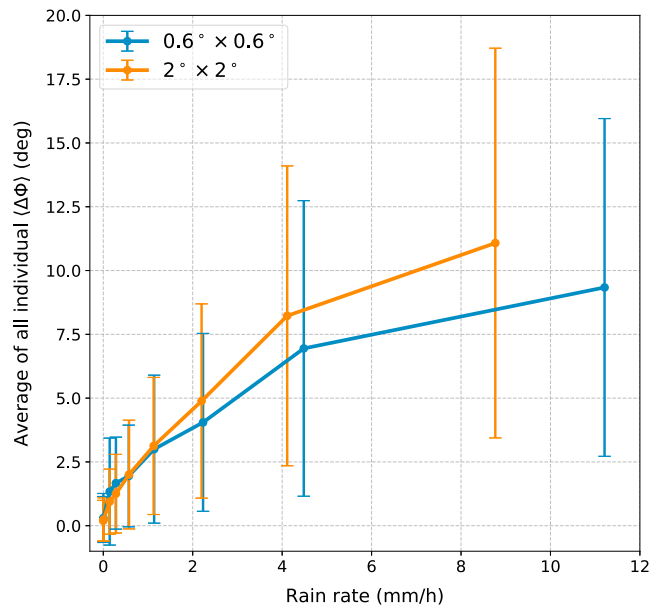


Figure 3. Mean polarimetric phase shift of individual profiles $\langle \Delta\phi \rangle_{0-20\text{km}}$ averaged in groups of similar rain rate. The binning in rain rate is not homogeneous to prevent large disparities in the population within each bin. For a given polarimetric phase difference, the mean precipitation in equator-equivalent $2^\circ \times 2^\circ$ cells is lower than the one in equator-equivalent $0.6^\circ \times 0.6^\circ$ cells. This result is consistent with parts of the large cell not registering any precipitation, while the $0.6^\circ \times 0.6^\circ$ cells are more likely to be within the precipitating rain cell at the polarimetric radio occultation tangent point.

be the origin of the polarimetric phase shift and supports the hypothesis that $\Delta\phi$ signals link to presence of hydrometeors. The link between the altitude where $\Delta\phi$ is predominant and the potential altitude of the precipitation cell is confirmed when we search the altitude of maximum polarimetric signal at each profile with $R_{0.6^\circ} > 2$ mm/hr and group them by CTH. As seen in Figure 4 (right), the higher the CTH the higher the altitude of the predominant ROHP-PAZ polarimetric phase shift, consistent with precipitation cells reaching higher altitudes.

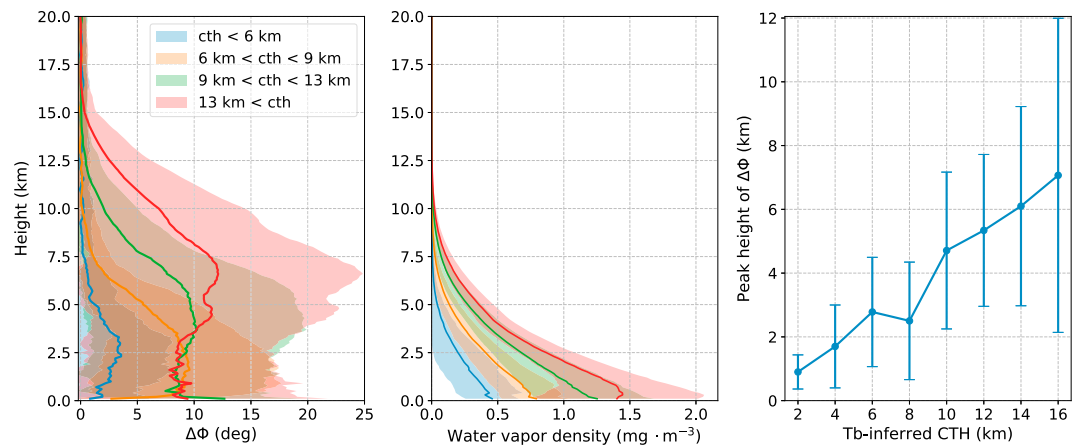


Figure 4. (left) Mean (solid line) and dispersion (shade) of four subsets of data, all correspond to cases with $R_{2^\circ} > 1$ mm/hr. They are grouped according to the estimated cloud top heights (CTHs) as shown in the legend. (middle) Mean (solid line) and dispersion (shade) of the observed Global Navigation Satellite System radio occultation water vapor density as function of the altitude, for the same subsets. (right) Average of the altitudes where the maximum $\Delta\phi(h_t)$ occurs as a function of the CTH, for cases with $R_{0.6^\circ} > 2$ mm/hr. A map with the geographic distribution of these events and their height of maximum polarimetric shift can be found in supporting information S3.

5. Discussion and Conclusions

This study describes a preliminary analysis of the first data set of PROs acquired from space by the ROHP-PAZ experiment during the five first months of its commissioning phase. Colocation with 2-D IMERG rain rate products and NCEP/CPC infrared brightness temperatures have been used to analyze the response of ROHP-PAZ observations. The coarseness of the colocation has introduced some dispersion into the statistics by either adding rain cells not crossed by RO rays within the spatial averaging (especially in $R_{2\sigma}$) or missing rain beyond it (e.g., along the RO plane in $R_{0.6\sigma}$). Despite this limitation, the statistics of the polarimetric phase shifts are shown to be linked to the presence of hydrometeors, with higher $\Delta\phi(h_t)$ in events of more intense rain. Moreover, the vertical distribution of the polarimetric phase shift is consistent with the height of the precipitation system, preliminary assessed using the CTH defined as the altitude of the RO temperature profile that matches the infrared brightness temperature of the scene. The conclusion of this study is that spaceborne GNSS PRO polarimetric phase shifts are sensing hydrometeors, with larger signals for heavier precipitation, confirming the theoretical studies in Cardellach et al. (2014) and Cardellach et al. (2017), the field campaign results of Padullés et al. (2016), and the predictions by Tomás et al. (2018).

The polarimetric shift in individual profiles often exceeds those predicted in simulation works (Cardellach et al., 2014; Cardellach et al., 2017), indicating that hydrometeors induce strong signals. This is most evident on the higher altitudes, where mixed phase and cloud ice might also contribute to the polarimetric signals. The differences with the simulations could also be partially due to the coarse colocation used in the present study, which averages the IMERG rain rate over large areas, or to underestimation in the models used in the simulation studies. Consequently, we will need to recalibrate the retrieval tools developed in the past based on synthetic data (lookup tables presented in Cardellach et al., 2017). Accumulation of additional ROHP-PAZ data will enable us to refine the retrieval tools and improve the instrumental calibration (including studies on the different degree of ellipticity present in transmitted signals) and further understanding on whether ionospheric effects might be having an impact on some individual profiles (statistical analysis does not show a dependency). Particular cases and outliers will be analyzed. The objective of these efforts will be to invert the individual $\Delta\phi(h_t)$ profiles into vertical profiles of precipitation probabilities (e.g., exceedance probability of precipitation). ROHP-PAZ observables and retrieved products will then be publicly available. Furthermore, the ability of PRO to provide refractivity profiles inside the precipitating clouds remains, which makes it the only space-based remote sensing technique able to sense precipitation within clouds and constraint, via refractivity profiles, the associated thermodynamic conditions (e.g., de la Torre Juárez et al., 2018). Therefore, ROHP-PAZ GNSS PRO data could be of interest to investigate relationships between thermodynamic patterns and heavy precipitation structures, as no other satellite technique senses both aspects of intense rain phenomena.

References

- Anth, R., Ector, D., Hunt, D., Kuo, Y., Rocken, C., Schreiner, W., & Yen, N. (2008). The COSMIC/FORMOSAT-3 mission: Early results. *Bulletin of the American Meteorological Society*, 89, 313–333. <https://doi.org/10.1175/BAMS-89-3-313>
- Cardellach, E., Padullés, R., Tomás, S., Turk, F. J., Ao, C. O., & de la Torre Juárez, M. (2017). Probability of intense precipitation from polarimetric GNSS radio occultation observations. *Quarterly Journal of the Royal Meteorological Society*, 144, 206–220. <https://doi.org/10.1002/qj.3161>
- Cardellach, E., Tomás, S., Oliveras, S., Padullés, R., Rius, A., de la Torre-Juárez, M., & Schreiner, B. (2014). Sensitivity of PAZ LEO polarimetric GNSS Radio-Occlusion Experiment to Precipitation events. *IEEE Transactions on Geoscience and Remote Sensing*, 53(1), 190–206. <https://doi.org/10.1109/TGRS.2014.2320309>
- de la Torre Juárez, M., Padullés, R., Turk, F. J., & Cardellach, E. (2018). Signatures of heavy precipitation on the thermodynamics of clouds seen from satellite: Changes observed in temperature lapse rates and missed by weather analyses. *Journal of Geophysical Research: Atmospheres*, 123, 13,033–13,045. <https://doi.org/10.1029/2017JD028170>
- Duncan, D. I., & Kummerow, C. D. (2016). A 1DVAR retrieval applied to GMI: Algorithm description, validation, and sensitivities. *Journal of Geophysical Research: Atmospheres*, 121, 7415–7429. <https://doi.org/10.1002/2016JD024808>
- Intergovernmental Panel on Climate Change (2014). Evaluation of Climate Models. In *Climate Change 2013 – The Physical Science Basis: Working Group I Contribution to the Fifth Assessment Report of the Intergovernmental Panel on Climate Change* (pp. 741–866). Cambridge: Cambridge University Press. <https://doi.org/10.1017/CBO9781107415324.020>
- Greco, M., Olson, W., Munchak, S., Ringerud, S., Liao, L., Haddad, Z., & McLaughlin, S. (2016). The GPM combined algorithm. *Journal of Atmospheric and Oceanic Technology*, 33, 2225–2245. <https://doi.org/10.1175/JTECH-D-16-0019.1>
- Haddad, Z. S., Sawaya, R. C., Kacimi, S., Sy, O. O., Turk, F. J., & Steward, J. (2017). Interpreting millimeter-wave radiances over tropical convective clouds. *Journal of Geophysical Research: Atmospheres*, 122, 1650–1664. <https://doi.org/10.1002/2016JD025923>
- Holz, R. E., Ackerman, S., Antonelli, P., Nagle, F., Knuteson, R. O., McGill, M., et al. (2006). An improvement to the high-spectral-resolution CO₂-slicing cloud-top altitude retrieval. *Journal of Atmospheric and Oceanic Technology*, 23, 653–670. <https://doi.org/10.1175/JTECH1877.1>
- Huffman, G. (2017). GPM IMERG final precipitation L3 half hourly 0.1° × 0.1° V05. Greenbelt, MD: Goddard Earth Sciences Data and Information Services Center (GES DISC). Accessed: 08/20/2018, <https://doi.org/10.5067/GPM/IMERG/3B-HH/05>

Acknowledgments

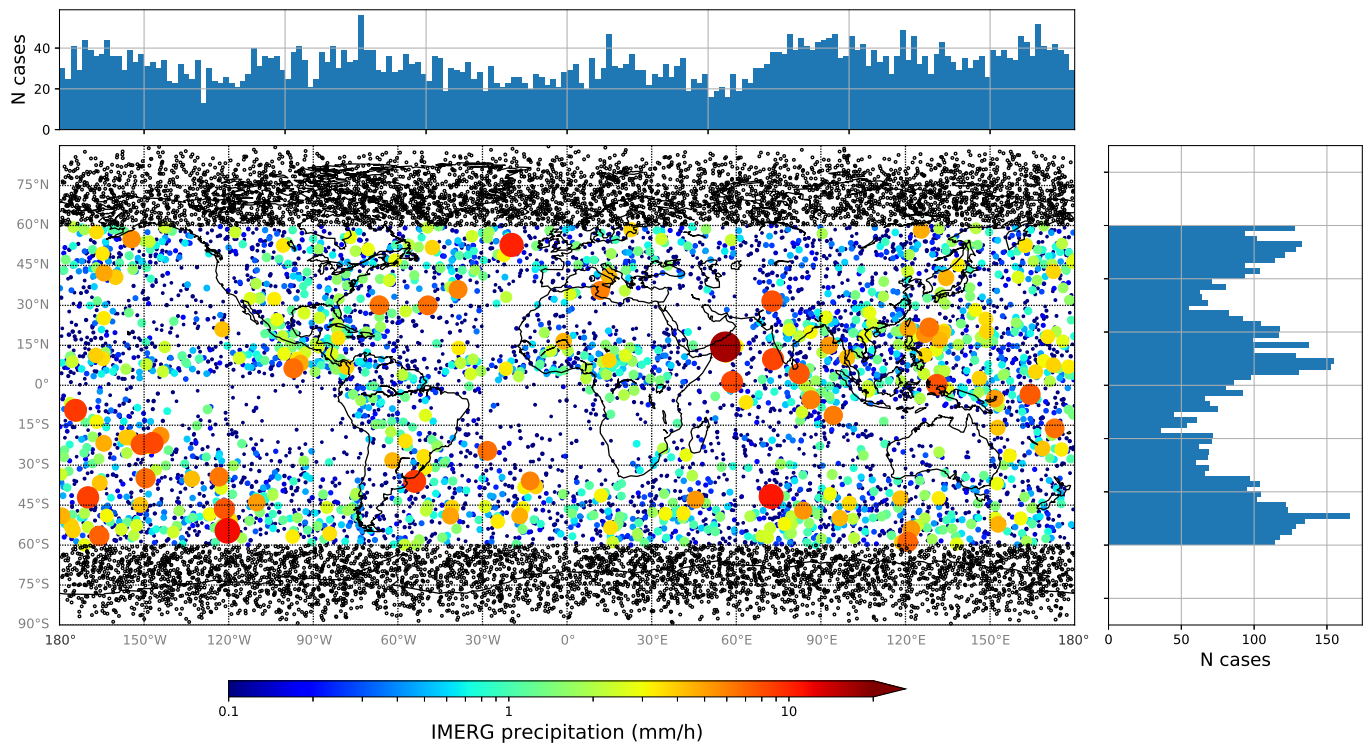
The ROHP-PAZ data used in this study are available at <https://paz.ice.csic.es/>. The colocations have been made on IMERG rain rates (Huffman et al., 2015; Huffman, 2017) and NCEP/CPC brightness temperatures (Janowiak et al., 2017); Figure 1 used GPM DPR data (Greco et al., 2016; Olson, 2017); all three sets are available at <https://disc.gsfc.nasa.gov/>. The ROHP-PAZ experiment is funded by the Spanish Ministry of Science, Innovation and Universities, currently under grant ESP2015-70014-C2-2-R. Work performed by C. O. A., G. W. F., B. A. I., D. K., T. K. M., R. P. M. T. J., and F. J. T. was carried out at the Jet Propulsion Laboratory, California Institute of Technology, under a contract with the National Aeronautics and Space Administration. JPL studies are supported by the NASA Earth Science U.S. Participating Investigator Program for the ROHP-PAZ mission, grant NNN14ZDA001N-ESUSPI. R. P. research was supported by an appointment to the NASA Postdoctoral Program at the Jet Propulsion Laboratory, administered by Universities Space Research Association under contract with NASA. The work performed by UCAR is supported by the National Oceanic and Atmospheric Administration National Environmental Satellite, Data, and Information Service.

- Huffman, G., Bolvin, D. T., Braithwaite, D., Hsu, K., Joyce, R., Kidd, C., & Xie, P. (2015). NASA Global Precipitation Measurement (GPM) Integrated Multi-satellite Retrievals for GPM (IMERG), Algorithm Theoretical Basis Document (ATBD) version 4.5.
- Janowiak, J., Joyce, B., & Xie, P. (2017). NCEP/CPC L3 Half Hourly 4km Global (60S-60N) Merged IR V1. In A. Savtchenko (Ed.). Greenbelt, MD: Goddard Earth Sciences Data and Information Services Center (GES DISC). Accessed: [last data access 01/10/2019], <https://doi.org/10.5067/P4HZB9N27EKU>
- Kuo, Y., Neelin, J. D., & Mechoso, C. R. (2017). Tropical convective transition statistics and causality in the water vapor-precipitation relation. *Journal of the Atmospheric Sciences*, *74*, 915–931. <https://doi.org/10.1175/JAS-D-16-0182.1>
- Kursinski, R., Hajj, G., Schofield, J., Linfield, R., & Hardy, K. (1997). Observing Earth's atmosphere with radio occultation measurements using the Global Positioning System. *Journal of Geophysical Research*, *102*(D19), 23,429–23,465.
- NASEM: National Academies of Sciences Engineering and Medicine (2018). *Thriving on our changing planet: A decadal strategy for Earth observation from space*. Washington, DC: The National Academies Press.
- Olson, W. (2017). GPM DPR and GMI combined precipitation L2B 1.5 hours 5 km V05. Greenbelt, MD: Goddard Earth Sciences Data and Information Services Center (GES DISC). Accessed: 08/20/2018, <https://doi.org/10.5067/GPM/DPRGMI/CMB/2B/05>
- Padullés, R., Cardellach, E., de la Torre Juárez, M., Tomás, S., Turk, F. J., Oliveras, S., & Rius, A. (2016). Atmospheric polarimetric effects on GNSS radio occultations: The ROHP-PAZ field campaign. *Atmospheric Chemistry and Physics*, *16*, 635–649. <https://doi.org/10.5194/acp-16-635-2016>
- Padullés, R., Cardellach, E., & Rius, A. (2016). Untangling rain structure from polarimetric GNSS Radio Occultation observables: A 2D tomographic approach. *European Journal of Remote Sensing*, *49*(1), 571–585. <https://doi.org/10.5721/EuJRS20164930>
- Schiro, K., Neelin, J., Adams, D., & Lintner, B. (2016). Deep convection and column water vapor over tropical land vs. tropical ocean: A comparison between the Amazon and the Tropical Western Pacific. *Journal of the Atmospheric Sciences*, *73*, 4043–4063. <https://doi.org/10.1175/JAS-D-16-0119.1>
- Sherwood, S., Hernández-Deckers, D., Colin, M., & Robinson, F. (2013). Slippery thermals and the cumulus entrainment paradox. *Journal of the Atmospheric Sciences*, *70*, 2426–2442. <https://doi.org/10.1175/JAS-D-12-0220.1>
- Smith, A., & Katz, R. (2013). US billion-dollar weather and climate disasters: Data sources, trends, accuracy and biases. *Nat Hazards*, *67*, 387–410. <https://doi.org/10.1007/s11069-013-0566-5>
- Sokolovskiy, S., Rocken, C., Schreiner, W., & Hunt, D. (2010). On the uncertainty of radio occultation inversions in the lower troposphere. *Journal of Geophysical Research*, *115*, D22111. <https://doi.org/10.1029/2010JD014058>
- Tan, J., Petersen, W., Kirstetter, P. E., & Tian, Y. (2017). Performance of IMERG as a function of spatiotemporal scale. *Journal of Hydrometeorology*, *18*, 307–319. <https://doi.org/10.1175/JHM-D-16-0174.1>
- Tomás, S., Padullés, R., & Cardellach, E. (2018). Separability of systematic effects in polarimetric GNSS radioccultations. *IEEE Transactions on Geoscience and Remote Sensing*, *56*(8), 4633–4649. <https://doi.org/10.1109/TGRS.2018.2831600>
- Zhao, M., Golaz, J., Held, I. M., Ramaswamy, V., Lin, S., Ming, Y., & Guo, H. (2016). Uncertainty in model climate sensitivity traced to representations of cumulus precipitation microphysics. *Journal Climate*, *29*, 543–560. <https://doi.org/10.1175/JCLI-D-15-0191.1>

Supplementary material to 'Sensing heavy
precipitation with GNSS polarimetric radio
occultations'

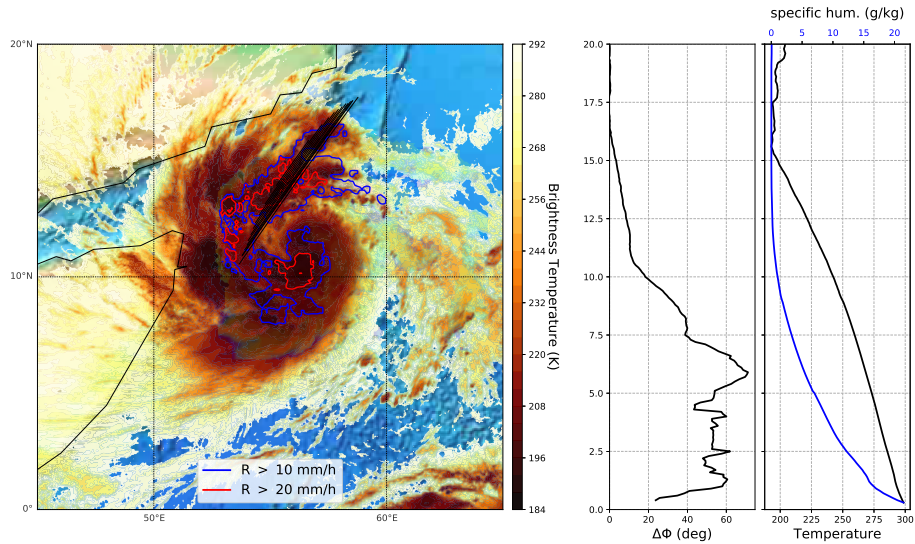
E. Cardellach et al.

December 7, 2018



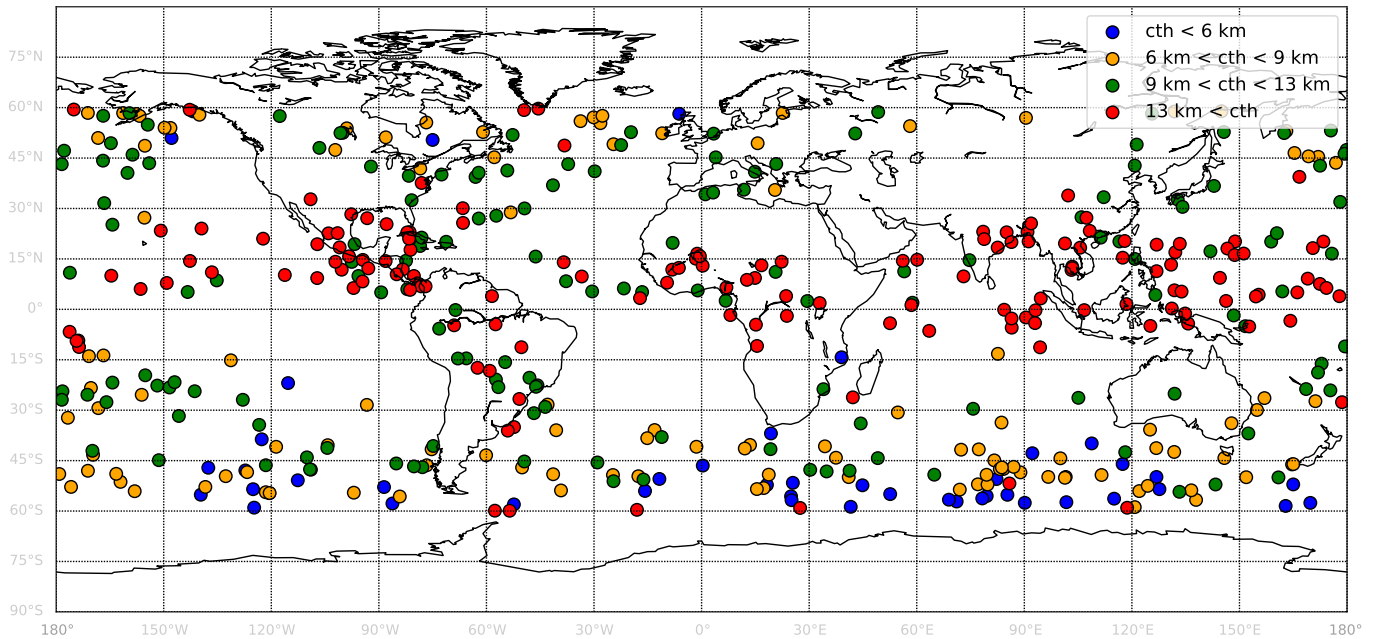
S1: geographic distribution of the rainy events

Geographic distribution of the ROHP-PAZ events acquired during the first five months of mission for which rain information is available through co-location with IMERG products, and for which IMERG rain rates around the RO averaged over an equator-equivalent $2^\circ \times 2^\circ$ are higher than $R_{2^\circ} > 0$ mm/h (colored dots). The size and color scale links to the co-located R_{2° . The black dots close to polar regions correspond to observation that do not present IMERG co-location. The histograms of latitudinal and longitudinal distribution correspond to IMERG co-located cases with $R_{2^\circ} > 0$ mm/h.



S2: extreme case in histogram Figure 2-right

Figure 2-right of the letter presents a case with a potential outlier value, with mean polarimetric shift $\sim 35^\circ$. As shown in the figure above, this outlier is not an artifact or instrumental error, but it corresponds to the sounding of an extreme event: a ROHP-PAZ profile crossing the bands of intense rain in a category-3 cyclonic storm, the Mekunu, occurring on the South-East of the Arabian Peninsula on May 23 2018 (3:04 UTC). The left panel above shows the co-located infrared image of the cyclone and its rain rate contour lines (solid colored contours), with indication of the ROHP-PAZ observation planes below 15 km altitude (black straight lines). The right panel shows the measured polarimetric shift $\Delta\phi(h_t)$ and the ROHP-PAZ derived temperature and specific humidity profiles.



S3: geographic distribution of the cases in Figure 4

The panel above shows the distribution of the cases in Figure 4-left and 4-center, all of them correspond to cases with $R_{2^\circ} > 1$ mm/h. They are grouped according to the estimated cloud-top heights as shown in the legend.

The top panel in the figure next page shows the geographic distribution of the ROHP-PAZ events presented in Figure 4-right of the letter. They correspond to cases for which the co-located IMERG rain rate averaged over equator-equivalent $0.6^\circ \times 0.6^\circ$ cells are equal or higher than $R_{0.6^\circ} > 2$ mm/h. The size of the dots corresponds to rain rate (see legend) whereas the color scale indicates the cloud-top height estimated by combination of the IR brightness temperature and the RO temperature profile. The figure on the bottom compiles the distribution and cloud-top height for cases with $R_{2^\circ} > 0.1$ mm/h.

